Ocean Engineering
Volume 108, 1 November 2015, Pages 129-139

ydrodynamic derivatives by RaNS simulation of planar motion mechanism test

Hyuncheol Kim, Hiromichi Akimoto, Hafizul Islam

https://doi.org/10.1016/j.oceaneng.2015.08.010

Highlights

- PMM simulation has been performed using an in-house RaNS solver for KCS model.
- Lateral force and yaw moment results have been compared with experimental data.
- Hydrodynamics force derivatives have also been calculated and compared.
- The results show high potential of RaNS solvers in- PMM simulation.

Abstract

Maneuverability prediction in design phase is one of the key requirements in ship design to ensure safety and economy of the ship. Generally, researchers and designers rely on towing tank tests to determine ship maneuverability properties and force derivatives. This paper discusses the possibility of applying Computational Fluid Dynamics (CFD) as an alternate to towing tank test for predicting ship maneuverability properties along with hydrodynamic derivatives using a RaNS based solver. The paper includes Planar Motion Mechanism (PMM) test results produced using CFD and compares the results with two sets of test data. It also discusses the derivation of force derivatives from the simulated PMM results and compares them with test ones. The results show good agreement in static drift and pure sway cases. As for pure yaw case, some discrepancy is observed, which may be attributed to the insufficiency of test data. The paper concludes that, CFD shows high promise as an efficient and economical alternative to existing towing tank tests in determining ship hydrodynamic coefficients.

Keywords

Computational fluid dynamics (CFD); Planar motion mechanism (PMM); Hydrodynamic derivatives; Towing tank test

1. Introduction

Ships are getting larger and faster with time, and accordingly, the importance of ship maneuverability prediction in design stage is increasing as well (Michio et al., 2009). After a ship is built, it is difficult to revise or change its maneuverability characteristics. The ocean accidents cause loss of life and property, sometimes they also damage ocean environment. To minimize ocean accidents, International Maritime Organization (IMO) adopted "Standards for ship maneuverability" in 2002 (IMO, 2002). As reflected by these standards, maneuverability of ship is more considerable part for maintaining safe navigation. Thus, for the prediction of ship's safety, path-keeping and path-changing ability, the demand of predicting maneuverability coefficients is increasing. Determinations of hydrodynamic derivatives are essential to determine ship's stability (Zou, 2006) during voyage. In case of model test, there are several difficulties like time and cost for model preparation, size limitation of towing tanks and mechanical limitations regarding prediction of real ship maneuverability. Thus, Computational Fluid Dynamics (CFD) is gaining large popularity as an effective tool to solve these problems.

Related research in the field has been going on for quite a while. Ryan and Wayne (1977) investigated in experimental environment to attain ship hydrodynamic derivatives. But it is rare to use computational method as, asymmetric (full hull) tests are required to attain ship hydrodynamic derivatives through CFD and Computational methods still have limitations in performing asymmetric non-linear simulations. SIMMAN 2008 was the first to collect both Experimental Fluid Dynamics (EFD) and CFD data for forced motions from different researchers and provided a relative comparison among the results. While previous works demonstrated in SIMMAN 2008 were limited to predicting lateral force and yaw moment for forced motion, this research takes it to the next stage by applying PMM motion for determining hydrodynamic derivatives.

CFD is gradually attracting the interest of designers for hydrodynamic coefficients calculation. However, the application of CFD is still somewhat limited because of its high resource requirements. The target of the present research is to demonstrate that RaNS solvers are able to predict ship maneuverability in an economical and efficient manner.

2. Ship maneuvering equation of motion

2.1. Coordinate systems

Two coordinate systems are used in this solver, earth-fixed coordinate system and body-fixed coordinate system. Each fixed coordinate system represents positions as xo, yo and zo, where center is at mid-point of the ship. X and Y indicate forces in direction x and y respectively and N is moment in z direction. Here, x axis follows bow to sternward direction, y axis is positive in the starboard side and z axis is positive in upward direction.

2.2. Mathematical model

In this coordinate system, the equations of motion are as followed.

$$Xo=mx¨oGYo=my¨oGNo=Iz0Gφ¨ \quad (1)$$

where Xo and Yo are the components of external forces acting on the ship in the directions of xo axis and yo axis, respectively. No is the component of external moment about the zoG axis. m is the mass of the ship and IzG is the moment of inertia of the ship about zoG axis. x¨oG and y¨oG are the components of acceleration in the direction of xo axis and yo axis, respectively. φ¨ is the yaw angle acceleration.

Therefore, Xo, Yo and No are transferred into X,YandN with respect to the body fixed coordinate system as following:

$$X=Xocosφ+YosinφY=–Xosinφ+YocosφN=IzGφ¨ \quad (2)$$

And, velocity ẋoG and ẏoG with respect to earth-fixed coordinate system are described using surge (u) and sway (v) velocity as below.

ẋoG=ucosφ–vsinφẏoG=usinφ+vcosφ (3)

And, acceleration ẍoG and ÿoG with respect to earth-fixed coordinate system are shown below, where u̇andv̇ are surge and sway acceleration respectively.

ẍoG=u̇cosφ–v̇sinφ–uφ̇sinφ–vφ̇cosφÿoG=u̇sinφ+v̇cosφ+uφ̇cosφ–vφ̇sinφ (4)

Therefore, with respect to body-fixed coordinate system, force and moment are as below (Fig. 1).

X=m(u̇G–vGφ̇)Y=m(v̇G+uGφ̇)N=IzGφ̈ (5)

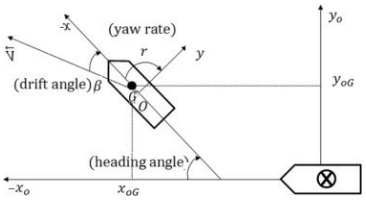

Download : Download high-res image (113KB) Download : Download full-size image

Fig. 1. Coordinate system.

Fig. 2 shows ship geometry about center of gravity and mid-ship point. From the mid-ship point, the location of center of gravity with respect to body-fixed coordinate system can be defined as xG,0,zG. And uG and vG can be changed in terms of um and vm.

uG=umvG=vm+xGφ̇ (6)

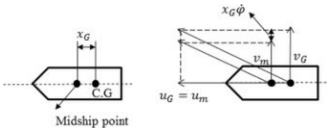

Download : Download high-res image (77KB) Download : Download full-size image

Fig. 2. Relation of geometry.

Also, body-fixed force X,Y and moment Nat center of gravity are changed in terms of mid-ship point's velocity and acceleration.

X=m(u̇G–vGφ̇)=m(u̇m–vmφ̇–xGφ̇2)Y=m(v̇G+uGφ̇)=m(v̇m+umφ̇+xGφ̈)N=Izφ̈+mxG(v̇m+uφ̇) (7)

Generally, two types of expression are used in describing the hydrodynamic force and moment. One is by Abkowitz (1969) and other is from Mathematical Modeling Group (MMG) in Japan. In case of Abkowitz method, hydrodynamic force and moment are expressed by using the Taylor series expansion. Hydrodynamic force and moment are expressed as functions of kinematical parameters and the rudder angle in the following form.

X=X(u,v,r,u̇,v̇,ṙ,δ)Y=Y(u,v,r,u̇,v̇,ṙ,δ)N=N(u,v,r,u̇,v̇,ṙ,δ) (8)

Since, the simulated ship model used in this research is bare hull, rudder term is omitted. And the kinematical parameters are expanded using Taylor series in the initial steady state with constant forward speed.

uo=U,vo=0,ro=0,u̇o=0,v̇o=0 and ṙo=0 are initial condition.

For convenience, the hydrodynamic derivatives for a certain nominal state are usually written as followed.

δXδu=Xu,δXδv=Xv,δXδr=Xr,δXδu̇=Xu̇,δXδv̇=Xv̇,δXδṙ=Xṙ (9)

Another method for expressing the hydrodynamic force and moment is from MMG. In the method, hydrodynamic force and moment consist of three parts, which are ship hull, propeller and rudder.

X=XH+XP+XRY=YH+YP+YRN=NH+NP+NR (10)

The subscripts "H", "P" and "R" denote the hull, propeller and rudder, respectively. In case of bare hull simulation, propeller and rudder parts are removed. Substituting Eq. (10) into Eq. (7), the equations of ship maneuvering motion are derived. This type of equation is called MMG model, or modular model. In this model, there are some assumptions. Maneuvering motions are small, therefore, higher-order terms in the expression of hydrodynamic force and moment are neglected. This results in the linear equations of ship maneuvering motion as follows.

X=m(u̇–vr–xGr2)=Xo+Xu(u–U)+Xvv+Xrr+Xu̇u̇+Xv̇v̇+Xṙṙ Y=m(v̇+ur+xGṙ)=Yo+Yu(u–U)+Yvv+Yrr+Yu̇u̇+Yv̇v̇+Yṙṙ N=Izṙ+mxG(v̇+ur)=No+Nu(u–U)+Nvv+Nrr+Nu̇u̇+Nṙṙ (11)

vr and xGr2 are very small, thus, for ensuring consistency, they are neglected. For the same reason, ur=(u–U+U)r=(u–U)r+Ur≈Ur. Likewise, at the initial steady state of forward ship motion, X,Y and N should vanish. Also, due to the ship symmetry, linear hydrodynamic derivatives Yu,Yu̇,Nu,Nu̇,Xv,Xv̇,Xr and Xṙ should be zero; as flow about the ship center plane remains symmetric. Assuming no controlling action, the control derivatives are also assumed zero.

Therefore, the equations can be simplified to:

(m–Xu̇)u̇–Xu(u–U)=0(m–Yv̇)v̇–Yvv+(mxG–Yṙ)ṙ+(mU–Yr)r=0(mxG–Nv̇)v̇–Nvv+(Iz–Nṙ)ṙ+(mxGU–Nr)r=0 (12)

Here, –Xu̇,–Yv̇,–Yṙ and –Nv̇ are called added masses. And –Nṙ is called added moment of inertia. Whereas, the coefficients –Xu,–Yv,–Yr,–Nv and –Nr are called damping coefficients (Zou 2006).

3. Model ship description

The model ship used for this research is the KRISO Container ship (KCS). It is a 3600TEU capacity container ship designed by KRISO (formerly MOERI) for research purpose. The ship is a very popular test model, as many of its experimental and CFD test results are open to public and has been discussed in many workshops and conferences like Gothenburg 2000 (Lars et al., 2003), CFD workshop Tokyo 2005 (Takanori, 2005), SIMMAN 2008 (Simonsen and Frederick, 2008), Gothenburg 2010 (Lars et al., 2013) etc. The KCS model provides data for both explication of flow physics and CFD validation for modern container ships. Fig. 3, Fig. 4 show the hull shape and body plan of KCS model.

Download : Download high-res image (21KB) Download : Download full-size image

Fig. 3. Shape of KCS.

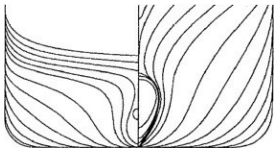

Download : Download high-res image (155KB) Download : Download full-size image

Fig. 4. Body plan of KCS.

For validation of CFD data, two different experimental data were used in this paper. The experimental data were provided by Hyundai Heavy Industries (HHI) and Changwon National University (CWNU). The basic dimensions of the model ships are in Table 1, along with the actual ship dimentions. The CFD simulation was performed in non-dimensional scale.

Table 1. Principal dimensions of KCS (actual and model ship).

	Actual	HHI model	CWNU model
Scale	1	40	322
Lpp (m)	230	5.75	0.7143
T (m)	10.8	0.27	0.0335
Bwl (m)	32.2	0.805	0.1
Displacement(m3)	52030	0.813	0.001558
CB	0.651	0.651	0.651
CM	0.985	0.985	0.985
LCG (m)	–3.4	–0.058	–0.01056
Ship speed (m/s)	12.35	1.952	0.69
Froude number (based of Lpp)	0.26	0.26	0.26
Reynolds number (based of Lpp)	2.1×109	8.4×106	3.7×105

4. The flow solver

The mathematical model of the solver, so called SHIP_Motion, has been elaborately discussed by Hideo and Hideaki (2003), and Hafizul (2015). The present research contributes to the solver by incorporating the PMM simulation model.

4.1. Mathematical model

4.1.1. Coordinate system

The SHIP_Motion follows two sets of coordinate system, body fixed (o-xyz) and earth-fixed (O-XYZ), defined in Cartesian system (Fig. 5). The earth fixed coordinate system is defined as, the O-XY plane being the still water plane and Z-axis being directed upwards. In body fixed coordinate system, the origin (0,0,0) lies at the center of gravity (c.g.) of ship and still water surface is at o-xy plane. For both the domains, the orientation of x-axis is from bow to stern ward direction, y-axis is positive towards starboard and z-axis is upward positive. For representation of the relative orientation system among the coordinate systems, Euler angles are used. The relation is described as following:

$$E(\emptyset,\theta,\varphi)=(\cos\theta\cos\varphi\cos\theta\sin\varphi-\sin\theta\sin\varphi\sin\theta\cos\varphi-\cos\emptyset\sin\varphi\sin\emptyset\sin\theta\sin\varphi+\cos\emptyset\cos\varphi\sin\emptyset\cos\theta\cos\emptyset\sin\theta\cos\varphi+\sin\emptyset\sin\varphi\cos\emptyset\sin\theta\sin\varphi-\sin\emptyset\cos\varphi\cos\emptyset\cos\theta) \quad (13)$$

$$(xyz)=E(\emptyset,\theta,\varphi)(XYZ) \quad (14)$$

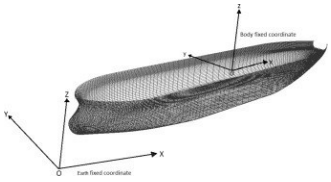

Download : Download high-res image (229KB) Download : Download full-size image

Fig. 5. Definition of coordinate system.

4.1.2. Governing equations

Governing equations are the three-dimensional, time-dependent, incompressible Reynolds average Navier–Stokes (RaNS) equation, and the continuity equation for fluid velocity and pressure. The RaNS and the continuity equations are expressed in the integral form for a control volume Ωc as:

$$\int\Omega c\delta u\delta t dV+\int\Omega c T dS=\int\Omega c K dV \quad (15)$$

$$\int\Omega c u\cdot dS=0 \quad (16)$$

where $\boldsymbol{u}$ is the fluid velocity vector, $\boldsymbol{T}$ is the fluid stress tensor and $\boldsymbol{K}$ is the body-force vector accounting for the inertial effect due to the motion of the coordinate system. The fluid stress tensor $\boldsymbol{T}$ is expressed as:

$$T=uu+\Phi I-(1Re+vt)[\nabla u+(\nabla u)T] \quad (17)$$

where, $\boldsymbol{I}$ is the identity tensor, Re is the Reynolds number, ∇ is the gradient operator, $(\cdot)^T$ denotes the transpose operator, and Φ is the piezo metric pressure excluding the hydrostatic pressure which is defined as:

$$\Phi=p+zFr2 \quad (18)$$

where, p is the static pressure and Fr is Froude number. The kinematic viscosity is evaluated by the turbulence model. The body force vector $\boldsymbol{K}$ is given as:

$$K=-2\omega\times u-\omega\times(\omega\times r)-d\omega dt\times r-dVdt \quad (19)$$

where ω is the angular velocity about the body-fixed coordinate system, $\boldsymbol{r}$ is the position vector to reference position, and $\boldsymbol{V}$ is the translation velocity vector of the ship in the directions of X, Y and Z.

4.1.3. Turbulence model

Three types of turbulence model are available in the SHIP_Motion. These are, the dynamic sub-grid scale (DSGS) model, the Baldwin–Lomax model (Bladwin and Lomax, 1978), and a hybrid of these two. For the PMM simulation, DSGS model has been applied for solving the outer mesh and Bladwin–Lomax model has been used for solving turbulence in inner mesh. DSGS is a modification of Smagorinsky model which allows Smagorinsky constant to vary in space and time. Bladwin–Lomax is a zero equation turbulence model. Bladwin–Lomax model is especially suitable for ship hydrodynamics as it places emphasize on quick design iteration.

4.1.4. Discretization

Spatial discretization is by the Finite Volume Method (FVM). The 3rd order upwind scheme is used for differencing for advection and 2nd order central difference for other discretizations in space. The definition of physical variables is in staggered manner, that is, the pressure is defined at the cell or volume center and the velocity quantities are defined at face centers.

In the solver, temporal discretization is by 2nd order Adams–Bashforth explicit method. As for parallel computing, SHIP_Motion uses OpenMP shared memory model.

4.1.5. Boundary condition

4.1.5.1. Free surface boundary condition

The kinematic condition for mass conservation is treated using the density-function method, where, ρ_m, which is a scalar variable, is defined in the entire computational region as:

$$\rho m=\{1 \text{fluid} 0 \text{otherwise} \tag{20}$$

This means that ρ_m is unity at any point fully occupied by the fluid, and changes from unity to zero above the free surface. In the control volume, including the free surface, the value of ρ_m is approximated by the fractional volume of the fluid that occupies the cell. Then the location of free surface is defined as the iso-surface of ρ_m=0.5. The time-dependent evolution of the density function is determined by solving the following transport equation of ρ_m.

$$\int\Omega c \delta \rho m \delta t dV=-\int\Omega c \rho m u \cdot dS \tag{21}$$

where, $\boldsymbol{u}$ is the fluid velocity. The right-hand side of the above equation is discretized using the QUICK scheme and temporal discretization is made by the second-order Adams–Molton method.

The dynamic condition is treated by extrapolating the velocity and the pressure above the free surface in a way that the surface tension and external stress on the free surface are ignored, and the zero-stress condition is approximately satisfied on the free surface.

4.1.5.2. Outer boundary condition

The definitions of the boundaries at the inner and outer domain are shown in Fig. 6, Fig. 7.

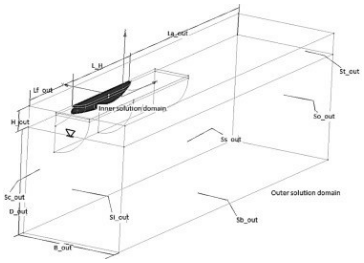

Download : Download high-res image (169KB) Download : Download full-size image

Fig. 6. Mesh boundaries, outer solution domain.

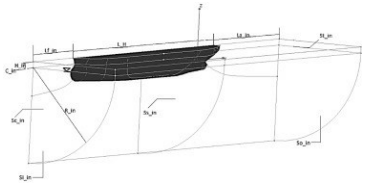

Download : Download high-res image (103KB) Download : Download full-size image

Fig. 7. Mesh boundaries, inner solution domain.

On the ship body (hull) boundary, the no-slip condition is imposed for fluid velocity. To reduce the requirement for high mesh resolution in the direction normal to the body surface, Spalding's universal wall function model has been employed. The body-boundary condition for pressure is derived by incorporating the no-slip condition for the velocity into the RaNS equation, and by assuming that the inner product of the diffusion term and the normal vector to the body surface is zero. The gradient of the density function normal to the body surface is assumed to be zero. Except for the case of zero advance velocity, a uniform flow is given at the inflow boundary of the outer solution domain (Si_outin Fig. 6). At the outflow and side boundaries of the outer solution domain (So_out, and Ss_out, respectively, in Fig. 6), the open-boundary condition is imposed for all the flow variables. At the center-plane boundaries (Sc_in and Sc_out in Fig. 6, Fig. 7), the symmetric condition is imposed for all the flow variables. At the inflow, outflow, and side boundaries of the inner solution domain (Si_in, So_in, and Ss_in, respectively, in Fig. 7), the Drichlet boundary conditions are obtained by interpolating the flow variables of the outer solution domain as described in the overlapping grid calculation (4.1.6).

4.1.6. Calculation for overlapping grid system

In the overlapping grid system, the flow computations are performed iteratively between the two grid systems and the flow information is exchanged by interpolating the flow variables at each boundary. During simulation, the inner grid moves according to the ship's motion and outer mesh only simulates free surface deformation. While simulation runs, the solver searches for the grid points located in the overlapping region of the two domains. Next, flow variables (velocity, pressure, density function) are interpolated from outer grid to overlapping inner grid locations. Flow in the inner grid is computed and updated. Again, the flow variables from the inner domain are interpolated to the overlapping outer grid locations. Flow variables at the outer domain are computed and updated. The process is repeated at every time step.

4.1.7. Pressure solution procedure

For a time-accurate solution of the incompressible flow, the divergence-free condition must be satisfied at each time-level. To achieve this, a Marker and Cell (MAC) type pressure solution algorithm is employed. The pressure is obtained by solving the Poisson's equation, using the Successive Over Relaxation (SOR) method. The velocity components are obtained by correcting the velocity predictor with the implicitly evaluated pressure.

4.1.8. Forced motion treatment for PMM

PMM motion is the combination of static drift, sway and yaw motions. In static drift, the ship moves through calm water with the yaw angle defined in input condition. For pure sway and pure yaw, ship follows sinusoidal motion following input amplitude and/or angle and period. The path function followed for yaw and sway motion are as followed:

$$\rho yaw=\beta \times \sin(2\pi \times(t-tpmmStart)/T) \rho sway=\eta sway \times \sin(2\pi \times(t-tpmmStart)/T) \tag{22}$$

In above equations, β represents yaw angle, t is the time, t_{pmmStart} is the PMM motion start time, T is PMM time period and ηsway is the sway amplitude.

4.1.9. Non-dimensionalization of parameters

All the fluid variables are made dimensionless with respect to the mean advancing velocity of the ship V_0, the ship length L, and the fluid density ρ. In the following equations, parameters on the left are dimension less ones and the starred ones on the right are with dimension.

time,t∗=t(VoL)

position,x∗=x(1L)

velocity,v∗=v(1vo)

acceleration,a∗=a(1vo2)

force,F∗=F(1ρVo2L2)

pressure,P∗=P(1ρVo2)

mass,m∗=m(1ρL3)

gravity,g∗=g(LVo2)=1Fn2

4.2. Computational mesh

In this research, an overset structured single block mesh system is used for simulation. The coarse rectangular outer mesh with high resolution around the free surface is used to capture the free surface deformation. The fine O–H type inner mesh around the hull surface is used for capturing the flow properties around the hull surface. *x–z* plane symmetry condition is used in head wave and calm water condition. As for captive model tests involving sway and yaw motion, full hull simulation is performed. In case of side and outflow boundaries, gradual higher spacing have been used for wave damping.

Fig. 8, Fig. 9, Fig. 10 show the fine inner mesh, coarse outer mesh and their combined arrangement, respectively. The specifications of the mesh used for PMM simulation, are in Table 2. Although mesh dependency has not been discussed in this paper, related discussion for the KCS and the KVLCC2 models can be found in the theses of Yu Bin (2014) and Hafizul (2015), respectively (Fig. 11).

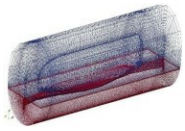

Fig. 8. Fine inner Mesh.

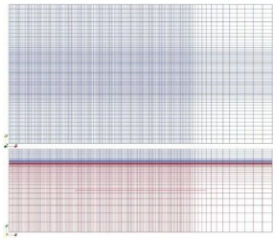

Fig. 9. Coarse outer mesh (top and front view).

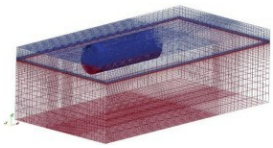

Fig. 10. Combined mesh assembly.

Table 2. Number of cells.

Mesh	Number of cells
Fine inner mesh (L=1.47, R=0.2)	356,000
Coarse outer mesh (L×B×D=3.8×1×1)	348,000
Total mesh	704,000

Fig. 11. Circulating water channel (CWNU).

5. Description of the experiment

Hyundai Heavy Industry (HHI) tested the KCS model in their towing tank facility and Hyeon-Kyu and Joo-Nyun (2010) from Changwon National University (CWNU) tested its KCS model in the circulating water channel. However, details on the experiments conducted by HHI are not entirely open to public (Table 3).

Table 3. Circular water tank specification.

Flow speed	**0.1–1.0m/s**
Total size	5000(L)×600(B)×2200(H) mm^3
Test section size	2000(L)×600(B)×500(H) mm^3
Amount of water	3 ton

6. Description of PMM motion and validation

The authors conduct the CFD simulation of Planar Motion Mechanism (PMM) test and derive hydrodynamic coefficients from the results. According to Gerler and Goodman, PMM test was introduced as an alternate to rotating arm test or circular motion test, where towing tank facility is longer and narrower. The PMM test uses model ship sinusoidal motions and it can determine coefficients- Yv,Nv,Yv̇, Nv̇, Yr,Nr, Yṙ and Nṙ.

PMM test imposes surge, sway and yaw motion on the test model. Static drift test, pure sway test and pure yaw test have been described in the following sections.

Using experimental data of HHI and CWNU, CFD results have been validated.

6.1. Static drift test

Fig. 12 shows motion of static drift test, from which, Yv and Nv are determined. Here, u and v indicate the partial differentiation for x- and y-axis velocity, respectively. Again, u̇ and v̇ indicate x- and y-axis acceleration, and r and ṙ are yaw rate and yaw acceleration, respectively. Definition of velocities and accelerations for static drift are described as below.

$$u=Vo\cos\beta, v=-Vo\sin\beta, r=0, \dot{u}=0, \dot{v}=0, \dot{r}=0, \quad (23)$$

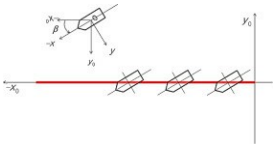

Download : Download high-res image (62KB) Download : Download full-size image

Fig. 12. Schematic diagram representing the motion of static drift test.

For validation, six static drift test cases were simulated. Simulated cases were for drift angle- 0°, 2°, 4°, 6°, 8° and 10°. HHI static drift cases were three, 0°, 6° and 10°, while CWNU tested eight cases, 0°, 2°, 4°, 6°, 8°, 10°, 12° and 15°.

$$Force'=Force\rho V2L2, Moment'=Moment\rho V2L3 \quad (24)$$

Fig. 13 shows the comparison between experimental and CFD results for tendency of Fy′ following drift angles. Although there are discrepancies among CFD, HHI and CWNU results, trend is almost the same. Up to drift angle of 6°, CFD results are almost same with experimental results, with an error level of 3%. In case of 8° drift angle, CFD produces a deviation of 15% with CWNU experimental data. However, as the general trend remains the same, CFD results can certainly be used for determining Fv hydrodynamics derivatives.

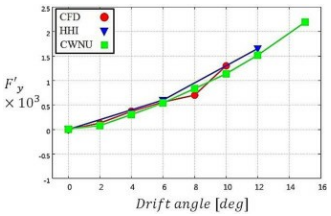

Download : Download high-res image (187KB) Download : Download full-size image

Fig. 13. Fy′ for varying drift angle.

Fig. 14 is the comparison of Mz′ for varying drift angle. Up to drift angle of 6°, CFD results are similar to experimental ones. However, after drift angle 6°, CFD and CWNU results show deviation comparing to HHI results (Fig. 15).

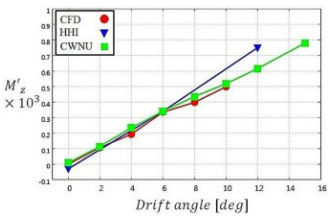

Download : Download high-res image (210KB) Download : Download full-size image

Fig. 14. Mz′ for varying drift angle.

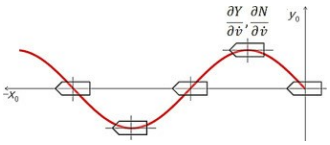

Download : Download high-res image (85KB) Download : Download full-size image

Fig. 15. Schematic diagram representing the motion of pure sway test.

6.2. Pure sway test

Pure sway test was used to determine derivatives of Yv̇ and Nv̇. Velocity u and v, acceleration u̇and v̇, yaw rate r and yaw acceleration ṙ are the same as in the static drift test case. Their relations are shown below.

u=Vo,v=ẏo,r=0,u̇=0,v̇=ÿo,ṙ=0,

$$y_o=\eta_{sway}\sin(\omega t+\varepsilon) \tag{25}$$

ηsway is sway amplitude and ω is frequency, which is 2πT. T is the period of one cycle. The maximum y-axis acceleration is ω2ηsway.

The velocity v is a sine function, at 90° phase difference with the displacement yo and the acceleration v̇; both of which are sine functions. Hence, the measurement of force Y is taken when the time variable has value 90° out of phase, with the displacement yo. These are forces arising from the effects of v and not from the effects of v̇, since the latter is zero at these times. In order to obtain the coefficients of the acceleration terms of Y-axis, Force Y must be measured, since v̇ is a maximum and v=0 (Lewis, 1988).

Thus, Yv̇ and Nv̇ are evaluated at the peak of sway force and moment. When ship is in zero sway amplitude, this force and moment indicates Yv and Nv. However, these derivatives can also be determined by static drift test. Generally, results through static drift are more correct and convenient to obtain.

Pure sway test is a dynamic test. Therefore, the measured forces and moments include the inertial force as followed.

$$Y=(Y\dot{v}-m)\dot{v}N=(N\dot{v}-mxG)\dot{v} \tag{26}$$

The inertia forces are considered here to keep the results comparable with experimental test results. The inertial effects should be taken into account in the estimation of dynamic derivatives as.

$$Y\dot{v}=1\dot{v}(Y+\dot{v}m)N\dot{v}=1\dot{v}(N+\dot{v}mxG) \tag{27}$$

Due to the different size of ship, it is essential to change from v̇ to non-dimensional form v̇′ by using Eq. (28).

$$-\dot{v}'=\dot{v}xLV2 \tag{28}$$

Here, L is length between perpendiculars, V is total velocity and is calculated as u2+v2. The minus sign before v̇′ is due to the reverse sign between position and acceleration.

Non-dimensionalization method for force and moment are same as in the static drift test. In pure sway test, twelve cases have been simulated. The sway acceleration (–v̇′max) are 0.01, 0.02, 0.05 0.08, 0.11, 0.13, 0.15, 0.19, 0.20, 0.28, 0.34 and 0.45. The non-dimensional time period for simulation was kept constant at 2. HHI produced three pure sway test cases with–v̇max: 0.1, 0.2 and 0.3. CWNU performed 4 case where –v̇max were 0.021, 0.084, 0.189 and 0.337.

Fig. 16, Fig. 17 show the CFD pure sway test time history of total lateral force Fy′ and yaw moment Mz′, respectively. In the figures, curve fitting to Fourier series has been used to generate smooth averaged curve. Hydrodynamic derivatives, Yv̇ and Nv̇ are determined by the force and moment values in the peak sway position (Lewis, 1988). In case of Yv̇, there is clear trend. But in case of Nv̇, it is independent of sway motion.

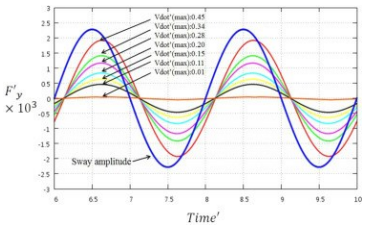

Download : Download high-res image (302KB) Download : Download full-size image

Fig. 16. CFD pure sway time history for total Fy′.

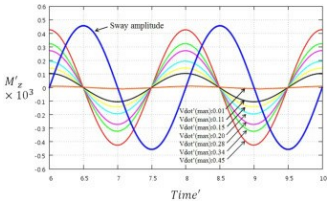

Download : Download high-res image (274KB) Download : Download full-size image

Fig. 17. CFD pure sway time history for total Mz′.

When ship is at the maximum sway displacement, according to v̇max′, Mz′ is almost zero. Also there is no clear trend in HHI and CWNU experiment data for Nv̇. A possible reason for this is too small force value to measure in the experiments.

Fig. 18 shows comparison of the tendency of Fy′ with respect to v̇max′. In all three data- CFD, HHI and CWNU results are almost the same with v̇max′ over –0.2. CWNU values are slightly different with CFD and HHI at low v̇max′, less than –0.3. Insufficiency of number of test data beyond that range may be among the reasons of mismatch. In common with static drift test, using CFD for pure sway test also shows high possibility and economic feasibility.

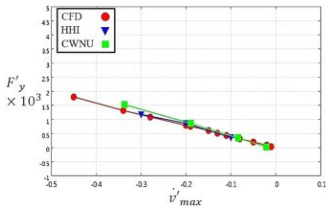

Download : Download high-res image (146KB) Download : Download full-size image

Fig. 18. Tendency of total Fy′ for v̇max′.

6.3. Pure yaw test

Fig. 19 depicts the motion of pure yaw test. Similar to the pure sway test, model ship is exposed to captive sinusoidal motion. Pure yaw results determine derivatives of Yṙ, Nr, Yṙ and Nṙ. Here, velocity u and v, acceleration u̇and v̇, yaw rate $r$and yaw acceleration ṙ are related in following manner.

u=Vocosφ+ẏosinφv=−Vosinφ+ẏocosφ≈0r=φ̇i=ÿosinφ−φ̇(Vosinφ−ẏocosφ)v̇=ÿocosφ−φ̇(Vocosφ+ẏosinφ)≈0ṙ=φ̈ (29)

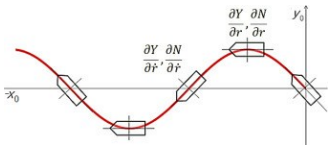

Download : Download high-res image (107KB) Download : Download full-size image

Fig. 19. Schematic diagram representing the motion of pure yaw test.

The formulations of φ is as below.

φ=φosin(ωt+ε)φo=tan−1(ωAvo),ε=π2 (30)

From Eq. (30), φ̇max and φ̈max can be determined. φ̇maxis ωφ0 and φ̈max is ω2φ0, where ω is frequency, which is 2π⁄T. T is the period of one cycle. The rotary derivatives, YṙandNṙ require the measurements when ṙ=0,v=0 and v̇=0. Similarly for Yṙ and Nṙ, the measurements must be taken when r=0,v=0 and v̇=0 (Lewis, 1988).

Thus, to determine Yṙ and Nṙ, force and moment have been calculated when yaw angle is at minimum. It is at zero instantaneous displacement, and when lateral displacement is maximum. Also to determine Yṙ and Nṙ, force and moment has been measured when yaw angle is in maximum displacement, and lateral or sway displacement (y_0) is minimum (which is zero). According to pure yaw motion, it should appear that when yaw angle is maximum, lateral displacement (y_0) will be zero and when yaw angle is zero, displacement amplitude will be maximum.

Pure yaw test is a dynamics test. Therefore, added mass term should be included to keep results comparable with test data. The formulation is shown below.

Y=(Yṙ−mu)ṙN=(Nṙ−mxGu)ṙY=(Yṙ−mxG)ṙ̇N=(Nṙ−Iz)ṙ̇ (31)

Again, inertial parts should be removed in the experimental data. Therefore, equations below are used.

Yṙ=1⁄ρ(Y+rmu)Nṙ=1⁄ρ(N+rmxGu)Yṙ=1⁄ρ(Y+ṙmxG)Nṙ=1⁄ρ(N+ṙIZ) (32)

r′ and ṙ′ are non-dimensionalized by Eq. (33).

r=rxLVṙ′=ṙxL2V2 (33)

Simulation cases for pure yaw motion with eight different yaw rates are shown in Table 4. HHI pure yaw test included three cases, where rmax′ were 0.3, 0.4 and 0.5; and CWNU performed six cases, with rmax′: 0.15, 0.20, 0.30, 0.40, 0.50 and 0.70.

Table 4. Simulation condition for pure yaw.

r′	ṙ′	T	Amp (Deg)
0.05	0.63	0.5	0.228
0.10	1.26	0.5	0.456
0.15	1.88	0.5	0.683
0.20	2.51	0.5	0.912
0.25	3.14	0.5	1.120
0.30	3.77	0.5	1.368
0.35	4.40	0.5	1.596
0.40	5.02	0.5	1.824

Pure yaw simulations also cover eight cases, as shown in Table 4. HHI pure yaw tests for ṙmax′ were three cases with –ṙmax′: 0.39, 0.61 and 0.86. and CWNU performed six cases for ṙmax′: 0.16, 0.29, 0.64, 1.14, 1.78 and 3.49.

Fig. 20, Fig. 21 show CFD pure yaw test time history of total Fy′ and total Mz′. In the figures, the curves have been fitted using Fourier series. To check clear change of peak value, total Fy′ and total Mz′ are presented consecutively. There is phase difference between yaw angle and sway displacement. Therefore, when yaw angle is at the peak, sway is zero. Also, when yaw angle is zero value, sway is maximum value. In case of total Fy′ peak value appears around yaw peak and sway is zero.

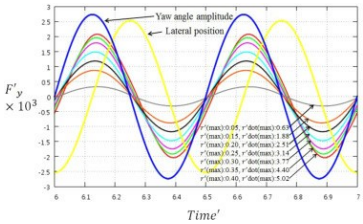

Download : Download high-res image (352KB) Download : Download full-size image

Fig. 20. CFD pure yaw test time history of total Fy′.

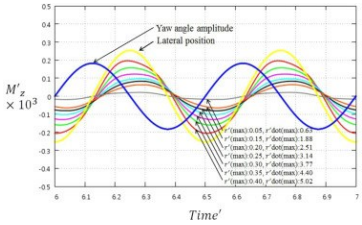

Download : Download high-res image (306KB) Download : Download full-size image

Fig. 21. CFD pure yaw test time history of total Mz′.

In case of total Mz′, peak value appear at around zero yaw angle and peak sway displacement. This fact is different with total Fy′. To determine derivatives Y_r and N_r Fy′ and Mz′ should be estimated in minimum yaw angle amplitude (Lewis, 1988). Except for that time, effect of yaw acceleration should be included. Also to determine derivatives Yṙ and Nṙ, Fy′ and Mz′ should be estimated at maximum yaw angle position (Lewis, 1988).

Fig. 22, Fig. 23 show comparison in CFD, HHI and CWNU results.

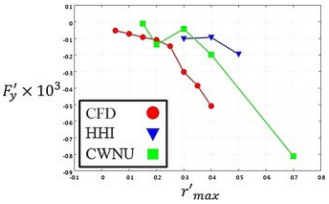

Download : Download high-res image (129KB) Download : Download full-size image

Fig. 22. Tendency of total Fy′ for rmax′.

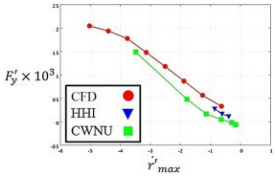

Download : Download high-res image (98KB) Download : Download full-size image

Fig. 23. Tendency of total Fy′ for ṙmax′.

Fig. 22 shows tendency of total Fy′ for rmax′. Although all results are in the same range, there are gaps among three results. In case of HHI and CWNU results, there is fluctuation in result value. According to rmax′ change, values of Fy′ should be straight line. So the trend of simulation result is more acceptable comparing with experimental data. In CWNU results, there is an abnormality at rmax′=0.3. The Fy′ value there should be lower than that at rmax′=0.2. Besides, the scaling effect may also be responsible for the discrepancy between the two tests as the model scale used by the two are different.

Also, the HHI result has an abnormality that the slope between rmax′=0.3 and 0.4 is positive which is different from the tendency of curves. These problems generally come from the higher non-linearity involved in pure yaw motion comparing to static drift and pure sway.

Fig. 23 shows tendency of total Fy′ for ṙmax′. The measurement range of HHI is very limited and some discrepancy exists between the results of CFD and CWNU. However, their trend is well captured.

These results indicate that it is possible that CFD can be a suitable substitute for model tests.

Fig. 24, Fig. 25 show tendency of total Mz′ for r′max and Mz′ for ṙmax′. In CFD results, values of Mz′ are very small comparing experimental results. Derivatives Nr and Nṙ are big values. In case of pure sway and pure yaw motion, there is a rapid change in flow from bow to stern direction. As, the lateral force and moment encountered is the sum of force and moment all through the hull surface, the changing flow pattern from bow to stern results into the non-linear predictions (Simonsen and Stern, 2008). Therefore, further investigation of CFD validation is required in the future.

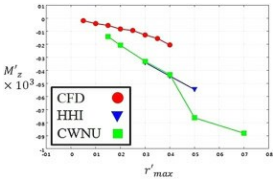

Download : Download high-res image (106KB) Download : Download full-size image

Fig. 24. Tendency of total Mz′ for rmax′.

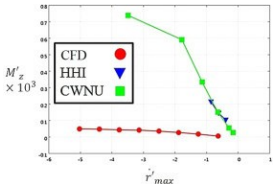

Download : Download high-res image (101KB) Download : Download full-size image

Fig. 25. Tendency of total Mz′ for ṙmax′.

7. Analysis of hydrodynamic coefficients

Ship hydrodynamic derivatives calculated using the CFD results are in Table 5, along with comparison of results derived from test data.

Table 5. Hydrodynamic derivatives and measuring efficiency.

	CFD (x103)	HHI (x103)	ε%	CWNU (x103)	ε%
Yv	0.108	0.130	17	0.125	14
Nv	0.051	0.061	16	0.053	4
Yv̇	3.90	4.10	5	4.48	13
Yr	1	0.33	203	0.86	16
Nr	0.435	1.10	60	1.27	65
Yṙ	0.44	0.31	42	0.37	19
Nṙ	0.01	0.247	96	0.241	96

Through static drift test, Yv and Nv are determined. And pure sway test provides Yv̇. Lastly, Yr, Yṙ, Nr and Nṙ are determined by pure yaw test. Hydrodynamic derivatives are estimated by regression analysis, and all projections are extended to (0,0) point with the assumption that these forces and moments are zero in static condition.

In case of Yv, discrepancy between CFD and HHI is 17%, and that between CFD and CWNU is 14%. Therefore, the present CFD results are acceptable in this level.

Result of Nv is better predicted comparing to Yv. Its difference between CFD and HHI is 16%, and that between CFD and CWNU is 4%. They are smaller than those of Yv. In case of CWNU results, values almost coincide with CFD values. Therefore, it is possible to determine derivatives Yv and Nv using CFD.

Derivative Yv̇ can be determined by using pure sway test. Result trend is better than Yv and Nv. Discrepancy between CFD and HHI is 5%, and between CFD and CWNU is 13%. Despite being dynamic test, derivative Yv̇ is quite close to experiment results. Considering the limitation of circulating water channel, it is possible to assume that HHI result is more close to real ship behavior. Therefore, with this point of view it can be suggested that CFD can determine derivative Yv̇ with good accuracy.

Derivatives Yr, Yṙ, Nr and Nṙ can be determined by using pure yaw test. Although trend of results are quite similar, level of discrepancy is big. By considering the limitation of circulating water channel, it is possible to assume that HHI results are closer to real ship behavior. However, pure yaw test is relatively non-linear, and proper measurement of rapidly changing flow pattern from bow to stern direction is quite critical. At the moment it is difficult to comment on the deviation. Thus, it can be stated that further work is needed in this part both in simulation section and comparison data section.

8. Computational resource

The simple solver with zero-equation Baldwin–Lomax turbulence model and the structured mesh around the bare hull, make the present simulation light and fast. However, the openMP memory sharing model used in the present simulation utilizes multi cores of only one node. Each simulations in this paper was performed in a single node of Intel(R) Xeon(R) CPU with 8 cores, clock speed 2.27 GHz and 8 GB of physical memory. The standard time step used was 1.0×10^{-4} non-dimensional time and for simulating each non-dimensional time, the required physical time was about 7 h per case. All the simulations were run up to 8 non-dimensional times for attaining stable results.

9. Conclusions

In this paper, the possibility of deriving ship hydrodynamic coefficients using CFD has been discussed and evaluated. The paper includes RaNS simulation results for PMM motion together with comparison with results of the model tests in towing tank and circular water channel. It also includes the comparison of ship hydrodynamic derivatives obtained from PMM simulation and tank tests. The basic construction of the solver and its meshing properties are in the paper.

The CFD results show reasonable agreement in case of static drift and pure sway simulations. The results indicate that RaNS simulation holds good possibility for forced motion simulations and can produce reasonably reliable maneuverability information. As for pure yaw simulation, discrepancies are found among simulation and test results. However, as the number of test data available has been limited and discrepancies are observed among test data, their reliability may be uncertain.

As for the derivation of ship hydrodynamic derivatives from simulation results, the results show a deviation ranging from 4% to 96% for different derivatives. Therefore, some results need further investigations. However, if the purpose of simulation is just design evaluation, present level of accuracy might be enough for the relative comparison among design candidates.

Overall, the results are convincing enough to suggest that, RaNS simulation holds bright potential as an alternate to traditional model tests for predicting ship maneuverability properties.

Acknowledgments

This work was partially supported by Hyundai Heavy industry (HHI) and Daewoo Ship Building and Marine Engineering (DSME). Professor Yoon from Changwon National University also contributed significantly by providing experimental data and support.

Recommended articles Citing articles (30)

References

Abkowitz, 1969 M.A. Abkowitz
Stability and Motion Control of Ocean Vehicles
The MIT Press, Cambridge, Mass (1969)
Google Scholar

Bladwin and Lomax, 1978 B. Bladwin, H. Lomax
Thin-layer approximaiton and algebric model for separated turbulent flow
AIAA Pap., 78 (1978), p. 0257
Google Scholar

Yu Bin, 2014 Ock Yu Bin
Numerical Simulation of Added Resistance Around Ships in Regular Head Waves Using Overset Grids
Master's thesis

Department of Naval Architecture and Ocean Engineering, Pusan National University, South Korea (2014)
Google Scholar

Hafizul, 2015 Islam Hafizul
Prediction of Ship Resistance in Oblique Waves Using RaNS Based Solver
Master's thesis
Division of Ocean Systems Engineering, KAIST, South Korea (2015)
Google Scholar

Hyeon-Kyu and Joo-Nyun, 2010 Yoon Hyeon-Kyu, Kang Joo-Nyun
Planar motion mechanism test of the mobile harbor running in design speed in circular water channel
J. Navig. Port Res. Int. Ed., 34 (7) (2010), pp. 525-532
View Record in Scopus Google Scholar

IMO, 2002 IMO (International Maritime Organization). Standards for ship maneuverability. Ref. T4/3.01 MSC/Circ. 1053, 16 Dec 2002.
Google Scholar

Lewis, 1988 Edward V. Lewis (Ed.), Principles of Naval Architecture, vol. 3, The Society of Naval Architecture and Marine Engineers, United States (1988)

Lars et al., 2003 Larsson Lars, Stern Frederick, V. Bertram
Benchmarking of computational fluid dynamics for ship flows: the Gothenburg 2000 workshop
J. Ship Res., 47 (1) (2003), pp. 63-81
Google Scholar

Larsson et al., 2013 Larsson Lars, Stern Frederick, Visonneau Michel. CFD in Ship Hydrodynamics – Results of the Gothenburg 2010 Workshop. DOI 10.1007/978-94-007-6143-8_14, 2013.
Google Scholar

Michio et al., 2009 Ueno Michio, Yasuo Yoshimura, Toshiaki Tsukada, Hideki Miyazaki
Circular motion tests and uncertainty analysis for ship maneuverability
J. Mar. Sci. Technol. (2009)
Google Scholar

Hideo and Hideaki, 2003 Orihara Hideo, Miyata Hideaki
Evaluation of added resistance in regular incident waves by computational fluid dynamics motion simulation using an overlapping grid system
J. Mar. Sci. Technol., 8 (2003), pp. 47-60
Google Scholar

Ryan and Wayne, 1977 Coe Ryan, Neu Wayne
Virtual Planar Motion Mechanism Tests in a CFD Environment
Department of Aerospace and Ocean Engineering, Virginia Tech, United States (1977)
Google Scholar

Simonsen and Stern, 2008 Simonsen Claus D. Stern Frederick, 2008. RANS simulation of the flow around the KCS container ship in pure yaw. In: Proceedings of the SIMMAN 2008 workshop.
Google Scholar

Simonsen and Frederick, 2008 Simonsen Claus D., Stern Frederick, 2008. RANS simulation of the flow around the KCS container ship in pure yaw. In: Proceedings of the SIMMAN.
Google Scholar

Hino, 2005 Hino Takanori, 2005. In: Proceedings of the CFD Workshop, Tokyo, National Maritime Research Institute Japan; 2005.
Google Scholar

Zou, 2006 Zou Zaojian, 2006. Ship maneuvering and sea-keeping.
Google Scholar

View Abstract